Supplement of

Benchmarking Snow Fields of ERA5-Land in the Northern Regions of North America

Robert Sarpong[1], Ali Nazemi[1]

[1] Department of Building, Civil and Environmental Engineering, Concordia University, Montreal, H3G 1M8, Canada

Correspondence to: Ali Nazemi (ali.nazemi@concordia.ca)

S1. ERA5-Land snow variables

The snowpack in HTESSEL model is treated as a single layer cover over the soil, with thermal insulation, density and albedo properties. The model allows for the interception of liquid water into the snowpack and aging processes (see Dutra et al., 2010; Balsamo et al., 2011). SD, SC, and SWE are modelled using a detailed representation of snow accumulation, compaction, and melting processes driven by coupling mass and energy balance equations at the snow layer.

SWE is modelled by mass balance equation, in which snowfall is accumulated in the snow layer, and depleted by snowmelt, sublimation and snowmelt runoff:

$$SWE(t) = SWE(t-1) + P_{snow}(t) - M_{snow}(t) - S_{snow}(t) - R_{snow}(t) \quad (1)$$

In which $P_{snow}(t)$, $M_{snow}(t)$, $S_{snow}(t)$, and R_{snow} are snowfall, snowmelt, sublimation and runoff from melting snow, respectively. The snowmelt and sublimation are derived from the energy balance equation:

$$Q_{net}(t) = Q_{SW}(t) + Q_{LW}(t) + Q_{sens}(t) + Q_{latent}(t) - Q_{ground}(t) \quad (2)$$

In which $Q_{SW}, Q_{LW}, Q_{sens}, Q_{latent}$, and Q_{ground} are incoming shortwave and longwave radiations, as well as sensible, latent and ground heat fluxes. Within this representation, snowmelt occurs when Q_{net} is positive and calculated as:

$$M_{snow}(t) = \frac{Q_{net}(t)}{L_f} \quad (3)$$

In which L_f is the latent heat of fusion. Similarly, sublimation can be derived from Q_{latent} and the latent heat of sublimation, L_s:

$$S_{snow}(t) = \frac{Q_{latent}(t)}{L_s} \quad (4)$$

SD can be inferred from SWE, given the knowledge of snow density:

$$SD(t) = \frac{SWE(t)}{\rho_{snow}(t)} \quad (5)$$

In which $\rho_{snow}(t)$ is snow density. Freshly fallen snow has a low density, however it evolves in time due to metamorphism, compaction and melt:

$$\frac{\rho_{snow}(t+1) - \rho_{snow}(t)}{\Delta t} = C_1 \rho_{snow}(t) \times \left(T_{snow}(t) - T_{ref}\right) + C_2 P_{snow}(t) \cdot \frac{\rho_{snow}(t)}{\rho_{ice}} - C_3 M_{snow}(t) \quad (6)$$

In which, C_1, C_2, and C_3 are parameters that quantify rates of snow metamorphism, compaction and melt, respectively. C_1 represents sensitivity of snow density to temperature changes, derived from physical principles related to snow grain metamorphism and bonding. C_2 is a coefficient related to the compaction of snow under pressure, based on the mechanical properties of snow and its response to overburden weight; and, C_3 is a coefficient that quantifies the impact of melting on snow density, derived from the energy required for phase changes and the dynamics of liquid water movement through the snowpack. $T_{snow}(t)$ and T_{ref} are temperature of snowpack and reference temperature and ρ_{ice} is the density of ice. Within ERA5L framework, snow density is constrained to remain within [50 450] kg m^{-3} (ECMWF, 2018).

By having $SD(t)$, SC at the time *t* can be determined as:

$$SC(t) = \min\left(1, \frac{SD(t)}{0.1}\right) \quad (7)$$

S2. CMC snow depth and snow water equivalent

The CMC's analysis of SD and SWE starts with collecting the in-situ SD, as well as precipitation and temperature data from the forecast model, with which a simple snowpack model is forced. The simulation results of the snowpack model provide a first-guess estimate for SD based on the calculated SWE according to the mass balance as well as the estimated snow density (see Equations 1 and 5). The assumption for mass balance equation is that the entire precipitation occurs at temperature 0°C or less is snowfall. This proportion is decreases linearly up to +2°C, where all the precipitation will be in rain. Also, sublimation is not modelled directly but is taken out as a landscape-dependent proportion of SWE at each timestep. The density of new snowfall is assumed to be a function of air temperature after Hedstrom and Pomeroy (1998):

$$\rho_{snowfall}(t) = \begin{cases} 67.9 + 51.3\exp\left(\frac{T_{air}(t)}{2.6}\right) & T_{air}(t) \leq 0℃ \\ 119.2 + 20T_{air}(t) & T_{air}(t) > 0℃ \end{cases} \quad (8)$$

The increase in snow density at each time step is calculated using empirical function for snow aging for cold and warm snow, which are discriminated based on temperature threshold of -1℃. The hourly settling rate for cold snow (i.e., $T_{air}(t) < T_{melt}$) is based on Anderson (1976) as:

$$\rho_{snow}(t+1) - \rho_{snow}(t) = 600C_1\exp\left[-0.08\left(T_{melt} - T_{snow}(t)\right)\right] \times SWE(t) \times \exp(C_2\rho_{snow}(t)) \quad (9)$$

In which $C_1$is the snow setting rate at T_{melt}; $T_{snow}(t)$ is the temperature of snow at time *t*; and C_2 is an empirically derived constant. For warm snow (i.e., $T_{air}(t) > T_{melt}$), the snow density is recursively calculated as (Tabler et al., 1990):

$$\rho_{snow}(t+1) = \rho^*(t+1) - 200\exp\left[\frac{\log\left(\rho^*(t+1) - \rho_{snow}(t)\right)}{200}\right] - 0.01 \quad (10)$$

In which $\rho^*(t+1)$ is the upper bound, given the snow density at $SD(t)$:

$$\rho^*(t+1) = 700 - \left(\frac{20470}{SD(t)}\right)\left[1 - \exp\left(\frac{-SD(t)}{67.3}\right)\right] \quad (11)$$

The density starts from a low density and increases as it ages. As new snow falls, the density declines. The density in CMC analysis is bounded in [100 550] kg m^{-3} (Brown and Brasnett, 2010).

Snowmelt is calculated using a variable degree-day melt factor, which is a function of snowpack density and vegetation cover following Kuusisto (1984):

$$\gamma(t) = \begin{cases} 0.0104\rho_{snow}(t) - 0.70 & \text{if forested area} \\ 0.0196\rho_{snow}(t) - 2.39 & \text{if open area} \end{cases} \quad (12)$$

In which $\gamma(t)$ is the melt factor at time *t*. Accordingly the snowmelt can be calculated as:

$$M_{snow}(t) = \gamma(t)[T_{air}(t) - T_{melt}] + \frac{C_w Rain(t)T_{air}(t)}{L_f\rho_{ice}} \quad (13)$$

The first term refers to the melt driven by temperature and the second term denotes to the melt contributed by rainfall in which C_w is the heat capacity of water and $Rain(t)$ is rainfall at time *t*.

Equations 8 to 14 together provide a basis to calculate the first-guess estimate of SD. These estimates are then blended with the in-situ observation of SD and corrected using the Optimum Interpolation scheme, described by Brasnett (1999):

$$SD^*(t) = SD(t) + \sum_{i \in I} w_i \left(SD_{i,obs}(t) - SD_i(t) \right) \tag{14}$$

In which $SD_{i,obs}(t) - SD_i(t)$ is the difference between in-situ observation and the first-guess estimate at station *i* that is within 600 km from the center of the grid in which $SD(t)$ is calculated. w_i is the optimum weight for station *i*. The vector of weights **w** for all neighbouring stations *I* can be calculated as:

$$\mathbf{w} = (\mathbf{P} + \mathbf{O})^{-1}\mathbf{q} \tag{15}$$

Where **P** is the correlation coefficient matrix of first-guess error between all pairs of observation, **O** is the normalized covariance matrix of observational errors between all pairs of observations and **q** is the vector of correlation coefficients of the first-guess error between the observation and the grid in which $SD(t)$ is calculated. **P** and **q** are selected in a way that the spatial correlation depends only on horizontal and vertical separation with a distance of 120 km in the horizontal and 800 m in the vertical directions.

S3. MODIS snow cover data

The MODIS detects snow cover based on the distinct spectral reflectance characteristics of snow (Riggs et al., 2019). Snow strongly reflects in the visible part of the spectrum but absorbs the shortwave infrared radiation, making it easily distinguishable from other land surfaces. This classification is made using the Normalized Difference Snow Index (NDSI; Hall et al., 1995), derived from MODIS instrument on NASA's Terra satellite. NDSI in a given day *t* can be calculated as (Wang et al., 2022):

$$NDSI(t) = \frac{R_{green}(t) - R_{SWIR}(t)}{R_{green}(t) + R_{SWIR}(t)} \tag{16}$$

In which R_{green} and R_{SWIR} are the reflectance in the green and shortwave infrared bands respectively (Dozier, 1989). The pixel is classified as snow-covered if both the NSDI and reflectance in the visible band exceed specific thresholds. One key challenge here is that NDSI cannot distinguish between clouds and snow cover; therefore, there is a need for resolving clouds (see also Gafurov and Bárdossy, 2009). The cloud masking in MODIS snow cover products involves multiple spectral tests and uses data from the MODIS Cloud Mask Product (MOD35; Ackerman et al., 2010), which assesses the presence of clouds using a combination of visible, infrared, and near-infrared bands (Ricciardelli et al., 2009). The results of these individual tests are combined to categorize the state of cloudiness. The snow cover algorithm integrates this cloud information to ensure only clear-sky observations are considered. If a pixel is flagged as cloud-covered, no snow cover is determined for that pixel in that

day, and the area is marked accordingly (Riggs et al., 2019). Accordingly, the Fraction of Snow Cover (FSC) over a grid cell in a given day *t* can be calculated as (Salomonson and Appel, 2004, 2006; Masson et al., 2018; Yan et al., 2022):

$$FSC(t) = -0.001 + 1.45NDSI(t) \quad (17)$$

To upscale daily data to monthly, grids with low FSC or high cloud cover are eliminated. In addition, a daily data must have a cloud cover less than 30% to be included in the averaging. The contribution of daily observation to the monthly averaging is based on its fractions of clouds. If there is no day within a month that satisfies this criterion then the monthly averaging is not calculated and the data is tagged as missing (see Riggs et al., 2019).

S4. Supplementary figures

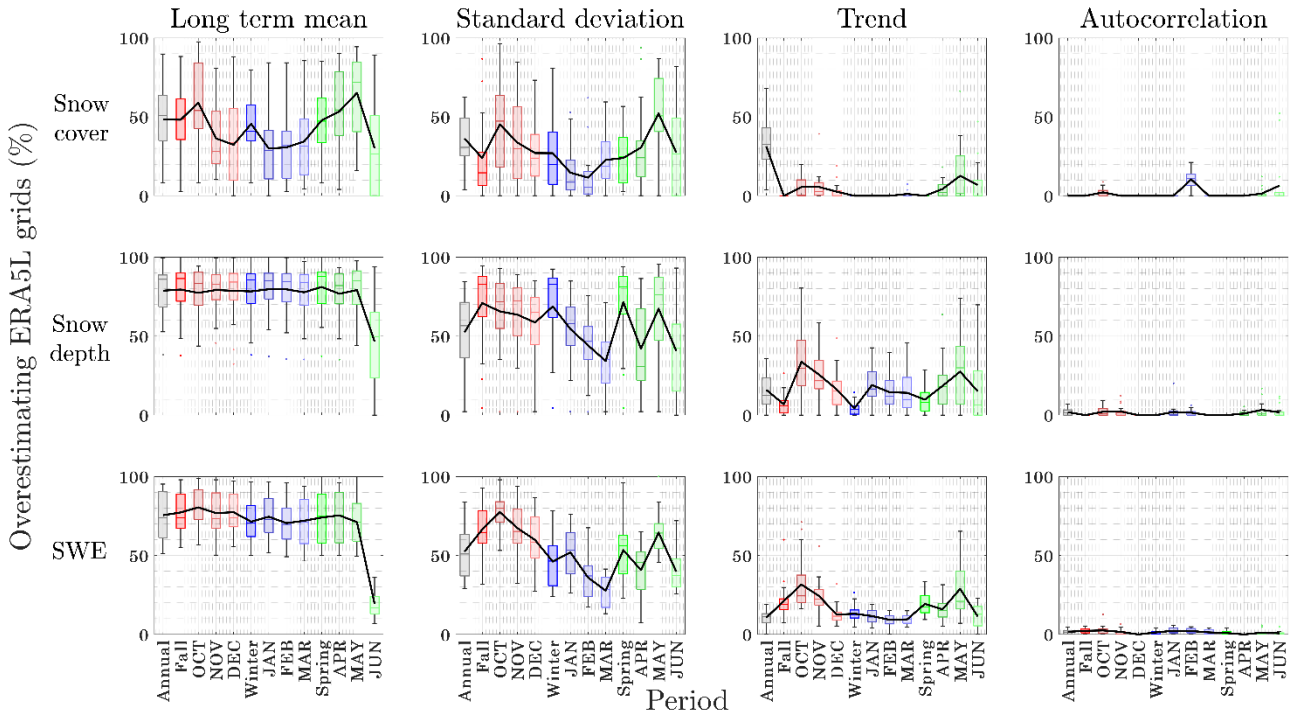

Figure S1: The temporal variations in the ratios of grids in which (from left to right) long-term mean, standard deviation, trend, and autocorrelation memory for snow cover (top row), snow depth (middle row) and Snow Water Equivalent (SWE; bottom row) are overestimated by ERA5-Land. The boxplots show the spatial variabilities in overestimated grids across 21 ecological regions, and solid lines depict the expected ratios of overestimated grids across the whole Canada and Alaska.

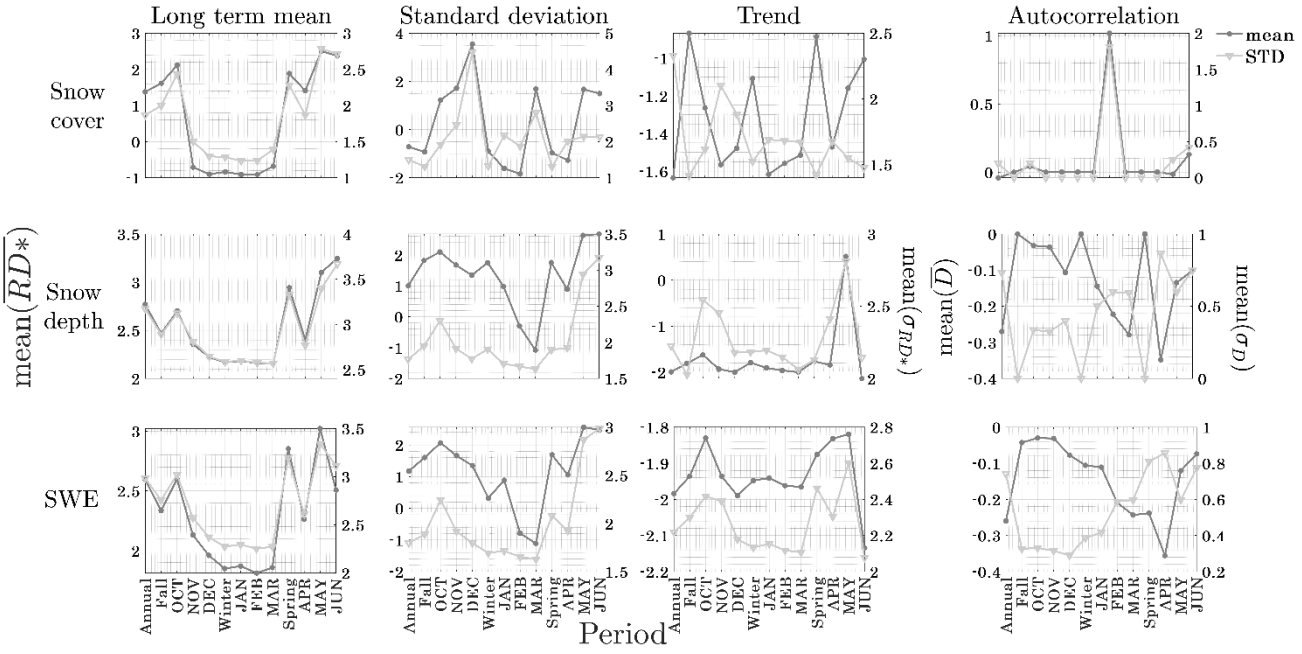

Figure S2: Temporal changes in expected mean (left *y* axis) and expected variabilities (right *y* axis) of regional discrepancies between ERA5-Land and reference products in (from left to right) long-term mean, standard deviation, trend and autocorrelation memory of snow cover (top row), snow depth (middle row) and Snow Water Equivalent (SWE; bottom row) across the 21 ecological regions

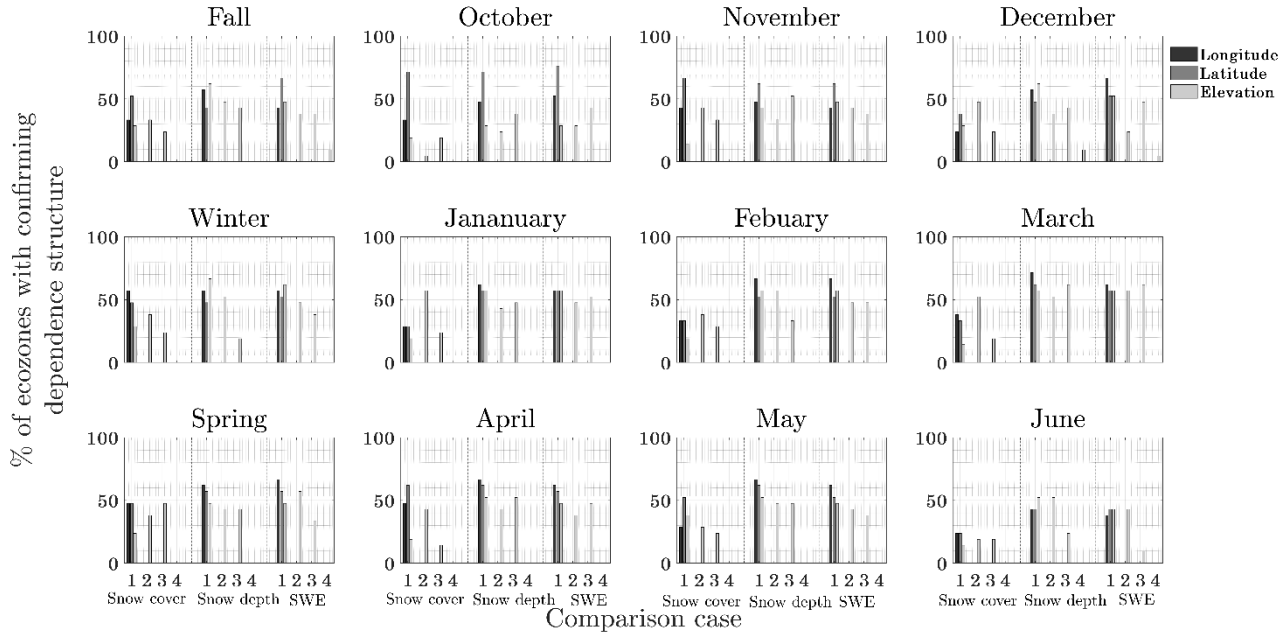

Figure S3: Ratios of ecological regions in Canada and Alaska for which spatial structures of snow characteristics inferred from ERA5-Land have strong similarity with reference products across different time scales. The spatial structures are estimated for four characteristics, i.e., (1) long-term mean, (2) standard deviation, (3) trend, and (4) autocorrelation memory of snow cover, snow depth and Snow Water Equivalent (SWE) with longitude, latitude and elevation.

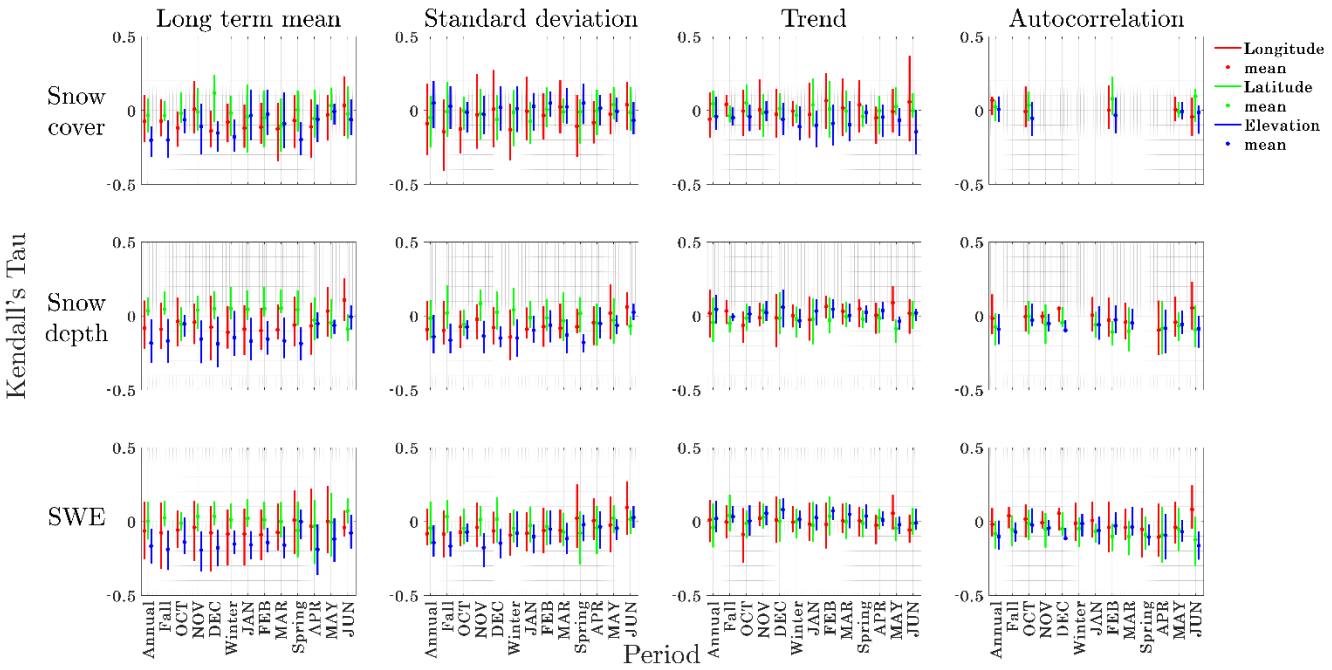

Figure S4: Interquartile ranges for annual, seasonal and monthly spatial dependencies of discrepancies in long-term mean, standard deviation, trend and autocorrelation memory of snow cover (top row), snow depth (middle row) and Snow Water Equivalence (SWE; bottom row) with longitude, latitude and elevation across 21 ecological regions in Canada and Alaska. Spatial dependencies are proxied by the Kendall's tau between discrepancies in estimates of the four characteristics with longitude (red), latitude (green), and elevation (blue). The expected values of spatial dependencies across the 21 ecological regions are marked with dots

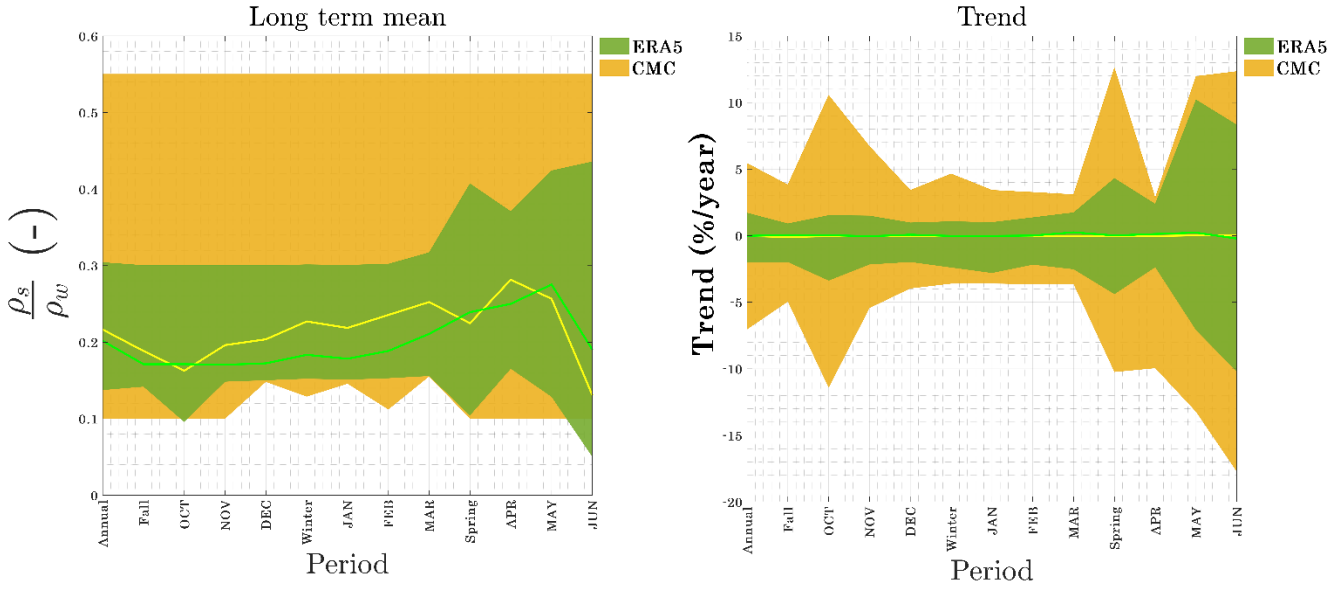

Figure S5: Temporal variations in the range of the gridded long-term means (left panel) and normalized trends (right panel) of snow-to-water density across Canada and Alaska obtained by ERA5-Land (green) and CMC (yellow) products. The expected values across the entire Canada and Alaska are shown by solid lines.

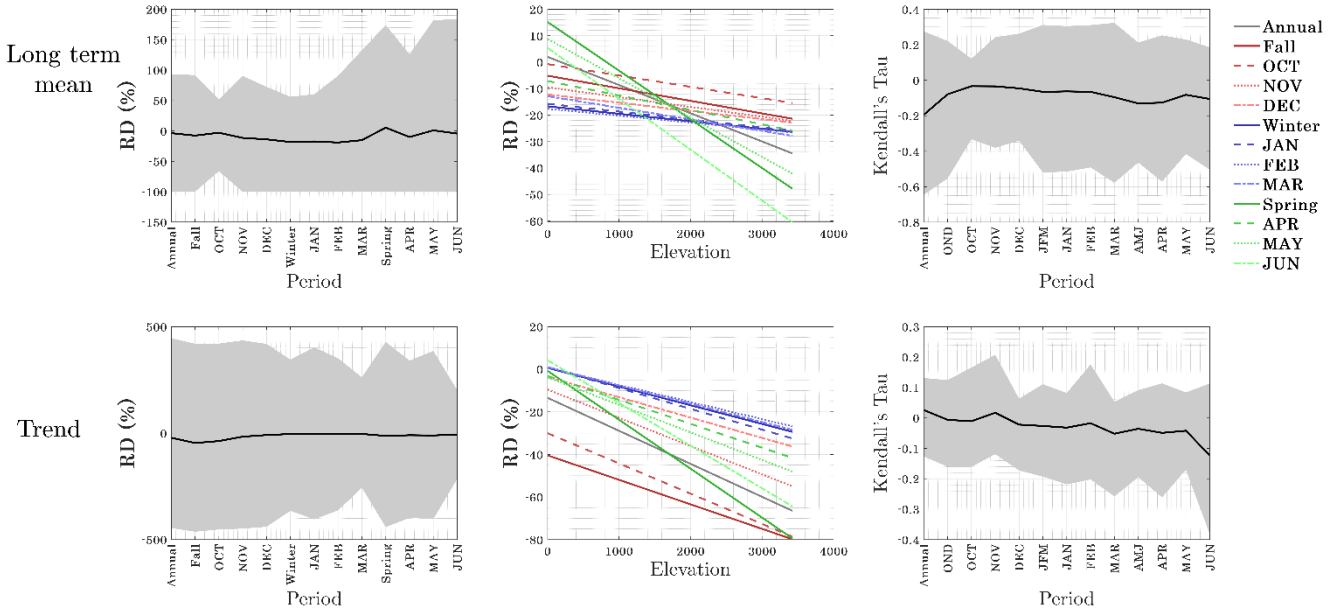

115 **Figure S6: (Left columns) temporal variations in the range of gridded discrepancies in estimates of long-term mean (top) and trend (bottom) in snow-to-water density. Solid black lines show the expected discrepancies across the entire Canada and Alaska. (Middle column) the variations in the role of elevation on monthly and seasonal discrepancies in estimates of long-term mean (top) and trend (bottom) in snow-to-water density. (Right column) the range of dependencies between gridded discrepancies and elevation across the 21 ecological regions of Canada and Alaska. The**
120 **expected dependencies are shown by solid black lines.**

References

Ackerman, S., Strabala, K., Menzel, P., Frey, R., Moeller, C., and Zhang, H.: Discriminating clear sky from cloud with MODIS algorithm theoretical basis document (mod35), https://citeseerx.ist.psu.edu/document?repid=rep1&type=pdf&doi=9c8d09b988e4f081d973ed46f2ada706613eb1a5, 2010.

125 Anderson, E. A.: A point energy balance model of a snow cover, NOAA Tech. Rep. NWS 19, Office of Hydrology, National Weather Service, available at: https://repository.library.noaa.gov/view/noaa/6392 , 150 pp., 1976.

Balsamo, G., Pappenberger, F., Dutra, E., Viterbo, P., and van den Hurk, B. J. J. M.: A revised land hydrology in the ECMWF model: A step towards daily water flux prediction in a fully-closed water cycle, Hydrol. Process., 25, 1046–1054, https://doi.org/10.1002/hyp.7800, 2011.

Brasnett, B.: A global analysis of snow depth for numerical weather prediction, J. Appl. Meteorol. Climatol., 38, 726–740, https://doi.org/10.1175/1520-0450(1999)038<0726:AGAOSD>2.0.CO;2, 1999.

Brown, R. D. and Brasnett, B.: Canadian Meteorological Centre (CMC) Daily Snow Depth Analysis Data, Version 1, Boulder, Colorado USA, NASA National Snow and Ice Data Center Distributed Active Archive Center, https://doi.org/10.5067/W9FOYWH0EQZ3 , 2010.

Dozier, J.: Spectral signature of alpine snow cover from the Landsat Thematic Mapper, Remote Sens. Environ., 28, 9–22, https://doi.org/10.1016/0034-4257(89)90029-4, 1989.

Dutra, E., Stepanenko, V. M., Balsamo, G., Viterbo, P., Miranda, P. M., Mironov, D., and Schär, C.: An offline study of the impact of lakes on the performance of the ECMWF surface scheme, Boreal Environ. Res., 15, 100, 2010.

ECMWF: IFS Documentation CY45R1 - Part IV: Physical processes, in IFS Documentation CY45R1, https://doi.org/10.21957/4whwo8jw0, 2018.

Gafurov, A., and Bárdossy, A.: Cloud removal methodology from MODIS snow cover product, Hydrol. Earth Syst. Sci., 13, 1361–1373, https://doi.org/10.5194/hess-13-1361-2009 , 2009.

Hall, D. K., Riggs, G. A., and Salomonson, V. V.: Development of methods for mapping global snow cover using moderate resolution imaging spectroradiometer data, Remote Sens. Environ., 54, 127–140, https://doi.org/10.1016/0034-4257(95)00147-2, 1995.

Hedstrom, N. R., and Pomeroy, J. W.: Measurements and modelling of snow interception in the boreal forest, Hydrol. Process., 12, 1611–1625, https://doi.org/10.1002/(SICI)1099-1085(19981015)12:10/11<1611::AID-HYP801>3.0.CO;2-Q, 1998.

Kuusisto, E.: Snow accumulation and snowmelt in Finland, Publ. Water Res. Inst., Natl. Board Waters, Finland, No. 55, 149 pp., available at https://helda.helsinki.fi/handle/10138/212849, 1984.

Masson, T., Dumont, M., Mura, M. D., Sirguey, P., Gascoin, S., Dedieu, J. P., and Chanussot, J.: An assessment of existing methodologies to retrieve snow cover fraction from MODIS data, Remote Sens., 10, 619, https://doi.org/10.3390/rs10040619, 2018.

Ricciardelli, E., Romano, F., and Cuomo, V.: A technique for classifying uncertain MOD35/MYD35 pixels through Meteosat second generation-spinning enhanced visible and infrared imager observations, IEEE Trans. Geosci. Remote Sens., 48, 2137–2149, https://doi.org/10.1109/TGRS.2009.2024375, 2009.

Riggs, G. A., Hall, D. K., and Román, M. O.: MODIS snow products collection 6 user guide, National Snow and Ice Data Center, Boulder, CO, USA, 66, available at https://nsidc.org/data/mod10cm/versions/61#anchor-documentation, 2019.

Salomonson, V. V., and Appel, I.: Development of the Aqua MODIS NDSI fractional snow cover algorithm and validation results, IEEE Trans. Geosci. Remote Sens., 44, 1747–1756, https://doi.org/10.1109/TGRS.2006.874745, 2006.

Salomonson, V. V., and Appel, I.: Estimating fractional snow cover from MODIS using the normalized difference snow index, Remote Sens. Environ., 89, 351–360, https://doi.org/10.1016/j.rse.2003.11.012, 2004.

Tabler, R. D.: Estimating snow transport from wind speed record: Estimates versus measurements at Prudhoe Bay, Alaska, in 58th Annual Meeting of Western Snow Conference, pp. 61–72, 1990.

Wang, G., Jiang, L., Xiong, C., and Zhang, Y.: Characterization of NDSI variation: Implications for snow cover mapping, IEEE Trans. Geosci. Remote Sens., 60, 1–18, https://doi.org/10.1109/TGRS.2022.3156727, 2022.

Yan, D., Ma, N., and Zhang, Y.: Development of a fine-resolution snow depth product based on the snow cover probability for the Tibetan Plateau: Validation and spatial–temporal analyses, J. Hydrol., 604, 127027, https://doi.org/10.1016/j.jhydrol.2021.127027, 2022.